Design strategies to rhodamine analogue fluorophores for near-infrared II biological imaging applications

Chuangjun Liu[a]* and Colleen N. Scott [b]*

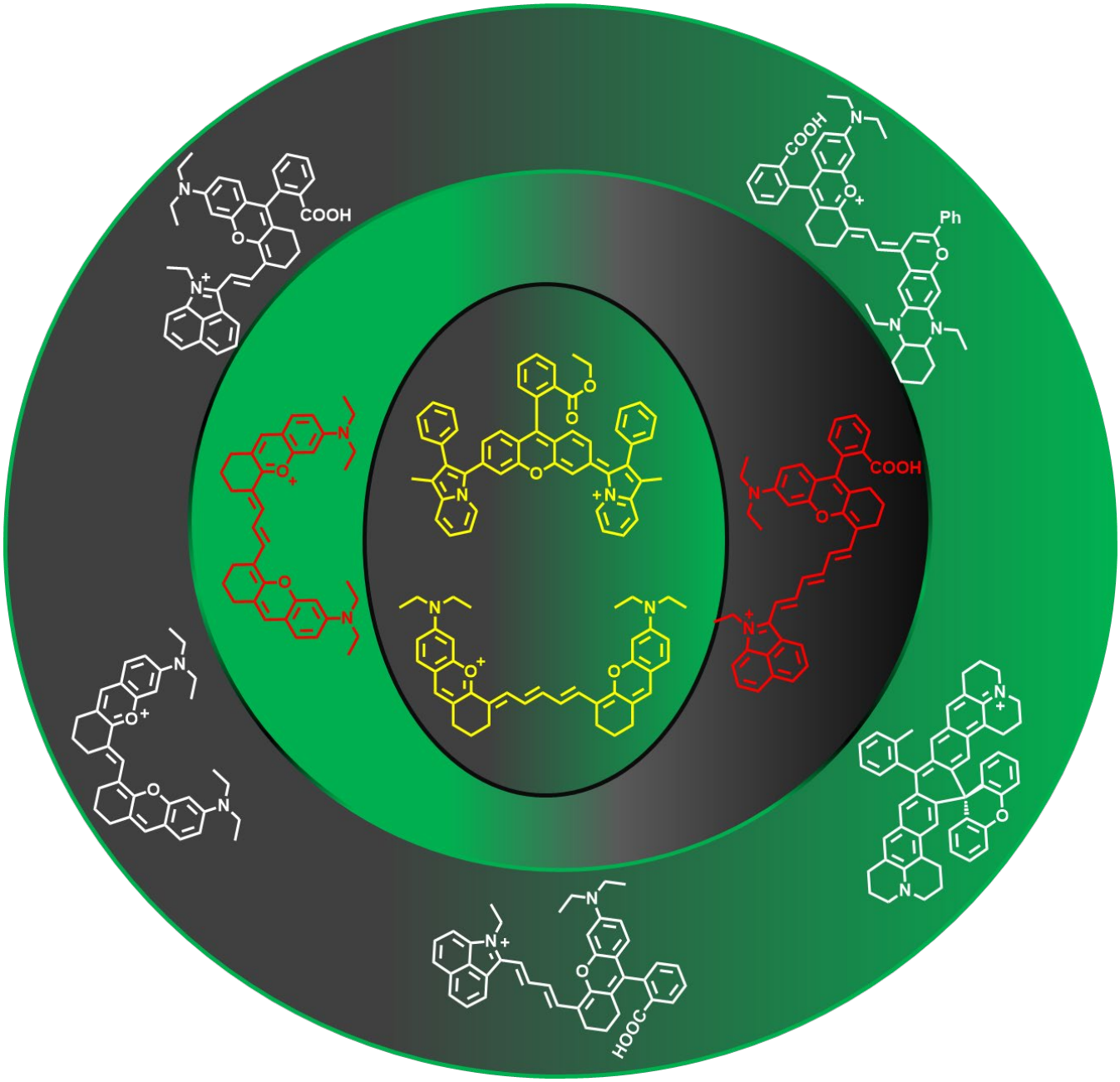

[a] Prof. CJ, Liu
Department of Chemistry and Pharmaceutical Engineering
Huanghuai University
Zhumadian, Henan, China 463000
E-mail: liuchuangjun@huanghuai.edu.cn
[b] Prof. CN Scott
Department of Chemistry
Mississippi State University
Mississippi State, MS 39762
E-mail: cscott@chemistry.msstate.edu

Abstract: Fluorescence imaging enables researchers to visualize a variety of biological tissues and processes with high spatial and temporal resolution. Near-infrared II (NIR-II) dyes are more desirable for imaging biological tissues than near-infrared I (NIR-I) dyes because of thier reduced light scattering and tissue autofluorescence, as well as deeper tissue penetration. Whilst the development of NIR-II absorption and emission fluorophores is challenging, some advances have been made in this area. For example, cyanine derivatives and donor-acceptor-donor (D-A-D) structures with a benzobisthiadiazole core are reported as common NIR-II fluorophores. Besides these NIR-II fluorophores, NIR-II rhodamine analogues are also being realized for biological applications due to their ability to combine imaging with sensing. In this mini-review, we summarize the molecular engineering design strategies, optical properties, and applications of NIR-II fluorophores developed from rhodamine analogues. Finally, our outlook for the future of this field is presented. We believe this review will reveal the progress made, but also some challenges in developing NIR-II rhodamine analogues for effective and efficient sensing and imaging in biological tissues. Consequently, this review will interest researchers from biomedical, environmental, and other dye related communities.

1. Introduction

Fluorescence imaging represents a powerful tool for visualizing a variety of biological processes due to its many advantages such as high spatiotemporal resolution, real-time detection, non-invasiveness, and low cost.[1-3] Fluorescence in the second near-infrared window (NIR-II), between 900-1700 nm, has been rapidly growing in recent years due to the deeper penetration of biological tissues (approximately 5-20 mm), reduced background autofluorescence, and improved signal-to-noise ratio (SNR) compared to the dyes in the visible (400-700 nm) and first near-infrared (NIR-I, 700-900 nm) window.[4-12] Therefore, the development of NIR-II imaging materials has attracted significant attention within the dye community. To date, materials used for NIR-II imaging can be classified into inorganic and organic. Inorganic materials include single-walled carbon nanotubes (SWNT), quantum dots, and rare earth metals doped nanoparticles. The organic materials are based on two types of architectures, donor-acceptor-donor (D-A-D) and polymethine cyanine fluorophore (Figure 1). Both the inorganic and organic materials mentioned above are summarized in several reviews.[13-18] However, those review articles did not comprehensively cover a third class of NIR II dyes, which is based on the xanthene core. NIR-II xanthene dyes based on the rhodamine structure have been an essential fluorophore for biological applications as they can be used for both sensing and imaging. Consequently, this article covers NIR-II organic fluorophores based on the rhodamine structure. Xanthene-based dyes, such as rhodamine and fluorescein, are classical fluorescent dyes with high photostability and fluorescent quantum yield, structures that are easily functionalized, and tunable luminescent properties.[19] Since their first discovery in 1887, various rhodamine dyes have been extensively studied as imaging with fluorescent markers or probes,[20-21] and a wide variety of rhodamine dyes have been commercialized. For

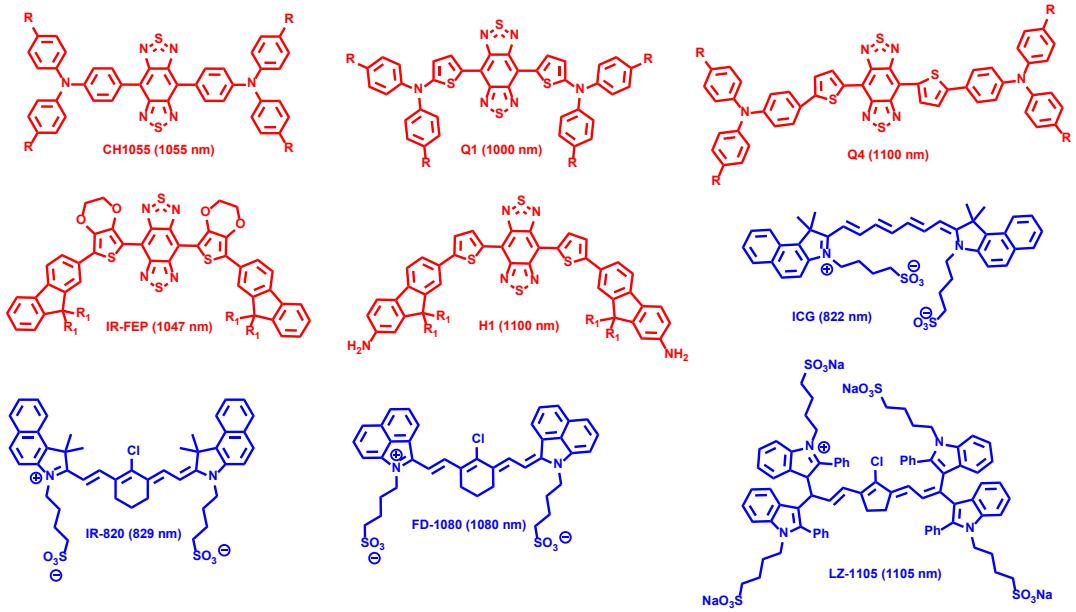

Figure 1. Representative D-A-D (in red) and polymethine cyanine (in blue) structures with their absorption wavelength in parentheses

Chuangjun Liu received his PhD degree (2016) from Southern Illinois University Carbondale (SIUC) under the leadership of Colleen Scott. He is currently a tenure-track Professor at Huanghuai University, where his research interests focus on the design and synthesis of photosensitizers and NIR-I/II fluorescent probes for biological applications.

Colleen Scott received her bachelor's degree in chemistry from Auburn University (1998) and her PhD from University of Pittsburgh (2005) in the field of organic chemistry. She began her independent career at Southern Illinois University Carbondale before transferring her research to Mississippi State University where she is an Associate Professor. Her research interests entail the design and synthesis of small molecules and polymeric materials for NIR-I/II probes, organic optoelectronic devices, and chemical upcycling.

example, commercially available rhodamine 123 is used as a mitotracker.[22] However, conventional rhodamine dyes absorb and emit in the visible region, which overlap with the absorption and emission of biological tissues. Conventional rhodamine dyes also have lower imaging penetration depth in tissues (< 1 mm) and high light scattering; thus, they produce low resolution images, which seriously hampers their applications *in vivo*.[23-24] Fluorophores with longer excitation wavelength in the NIR region generally provides increased optical penetration within tissues, improved SNR, and minimized cell damage, which are all great advantages for *in vivo* imaging.[25-27] Over the past decades, researchers have committed great effort to shift the absorption and emission wavelengths of rhodamine dyes into the NIR region.[28] Extending the conjugation of the xanthene core or replacing the central oxygen atom with other elements such as C,[29] S/Se,[30-31] P,[32] Si/Ge/Sn[33] and Te[34] are common strategies to red-shift the photoluminescence wavelengths of rhodamine dyes. However, these efforts have only led to dyes in the deep-red and NIR-I regions (Figure 2). Although NIR-I region is defined as the "biological transparent window", fluorescence imaging with NIR-I dyes still has the intrinsic issues of low tissue autofluorescence and marginal imaging depth (1-3.5 mm).[35] By contrast, fluorescence imaging with NIR-II dyes has significantly diminished the background noise and provides deeper tissue penetration depth (5-20 mm) due to the minimal photon scattering and low tissue absorption of NIR-II light.[8, 36] With these merits, fluorescence imaging with NIR-II dyes is able to visualize biological structures deep within tissues that are otherwise difficult to achieve for NIR-I dyes. As such, chemists have become inspired to develop novel rhodamine dyes that absorb and emit at wavelengths in the NIR-II region.

2. Synthetic strategies for NIR-II rhodamine fluorophores

Rhodamine 110, the simplest rhodamine dye, presents an absorption and emission maximum at 497 nm and 520 nm respectively, with a high quantum yield of 0.88 at emission

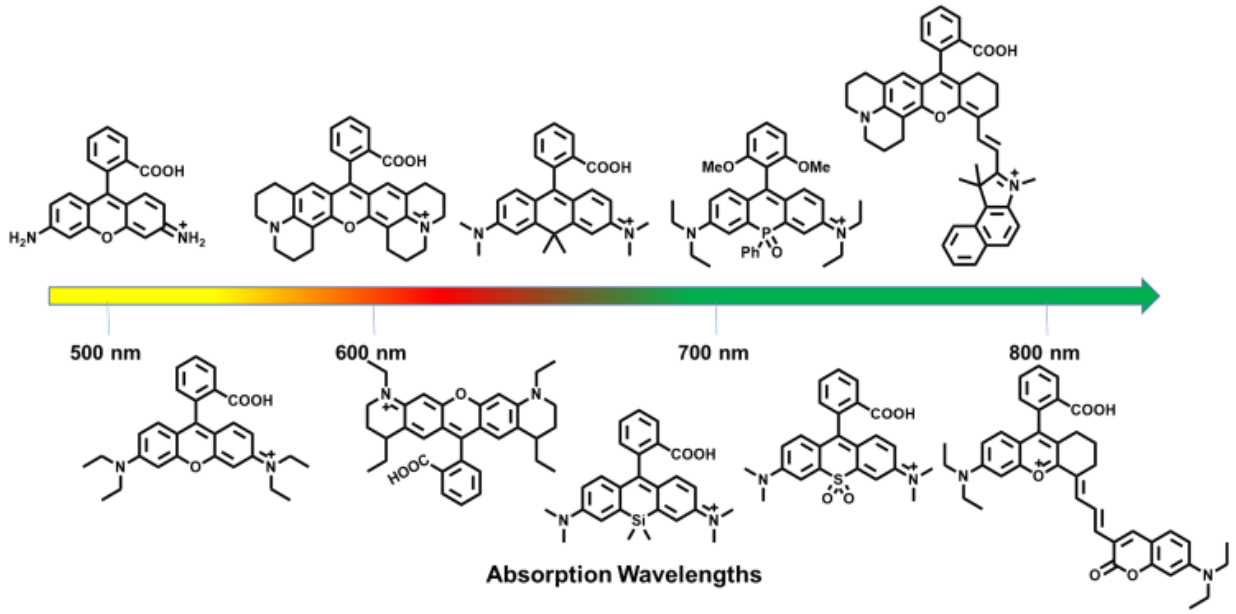

Figure 2. Absorption wavelengths of different rhodamine structure

maximum.[37] Modification of its amine groups can greatly decrease the energy gap between the highest occupied molecular orbital (HOMO) and lowest unoccupied molecular orbital (LUMO) resulting in longer absorption and emission wavelengths. For example, the julolidine structure of rhodamine fluorophore (λ_{abs} 580 nm, λ_{em} 600 nm) has around an 80 nm bathochromic shift compared to rhodamine 110.[38] Surprisingly, further extension in conjugation of the julolidine structure by two benzene rings causes more than 300 nm red-shift in the spectrum of the fluorophore, resulting in the λ_{abs} and λ_{em} in the deep NIR-I region. Yang *et al*., constructed a new class of rhodamine analogues based on the bisbenzo-C-rhodamine unit (ECX) as shown in Scheme 1.[39] While both ECXb in CH_2Cl_2 and ECXi in water showed maximum absorption wavelengths around 880 and 920 nm, respectively, their emission bands tailed in the NIR II region beyond 1100 nm (Figure 3a, b). This was the pioneering work of extending the wavelengths of rhodamine derivatives into the NIR-II window. The julolidine rings of ECX dyes prevent rotation around the nitrogen atoms; thus, they exhibited high fluorescence quantum yield (QY) in CH_2Cl_2 (7.6-13.3%), where the QY of ECXb reached up to 13.3%. Besides, ECX dyes were more photostable than the commercial dye, naphthalocyaine, which was used as a reference. **ECX** dyes are also chemically stable; for example, **ECXi** showed excellent chemostability in aqueous solutions at pH values between 3-12. Furthermore, only minimal changes were observed in the absorbance and fluorescence spectra of **ECXi** when exposed to biological sulfides, reactive oxygen species, and hydrogen peroxide. Strong fluorescent signals of **EXCb** were observed from the Hela cells and the mouse *in vivo* images (Figure 3c, d, e). However, the excitations of the **ECX** dyes series are still restricted to the NIR-I region and the emission tail beyond 1000 nm was very low. Inspired by indocyanine green (ICG) polymethine skeleton, Zhang *et al*., developed a series of NIR-II rhodamine version of the polymethine dyes (**CX**) via a one-step condensation reaction between compound **1** and electrophiles **2**, **3**, and **4**, yielding **CX-1**, **CX-2** and **CX-3**, respectively (Figure 4A).[40] As the conjugation length of the fluorophore increases from **CX-1** to **CX-3**, a bathochromic shift of about 100 nm in both the absorption and emission wavelengths was observed (Figure

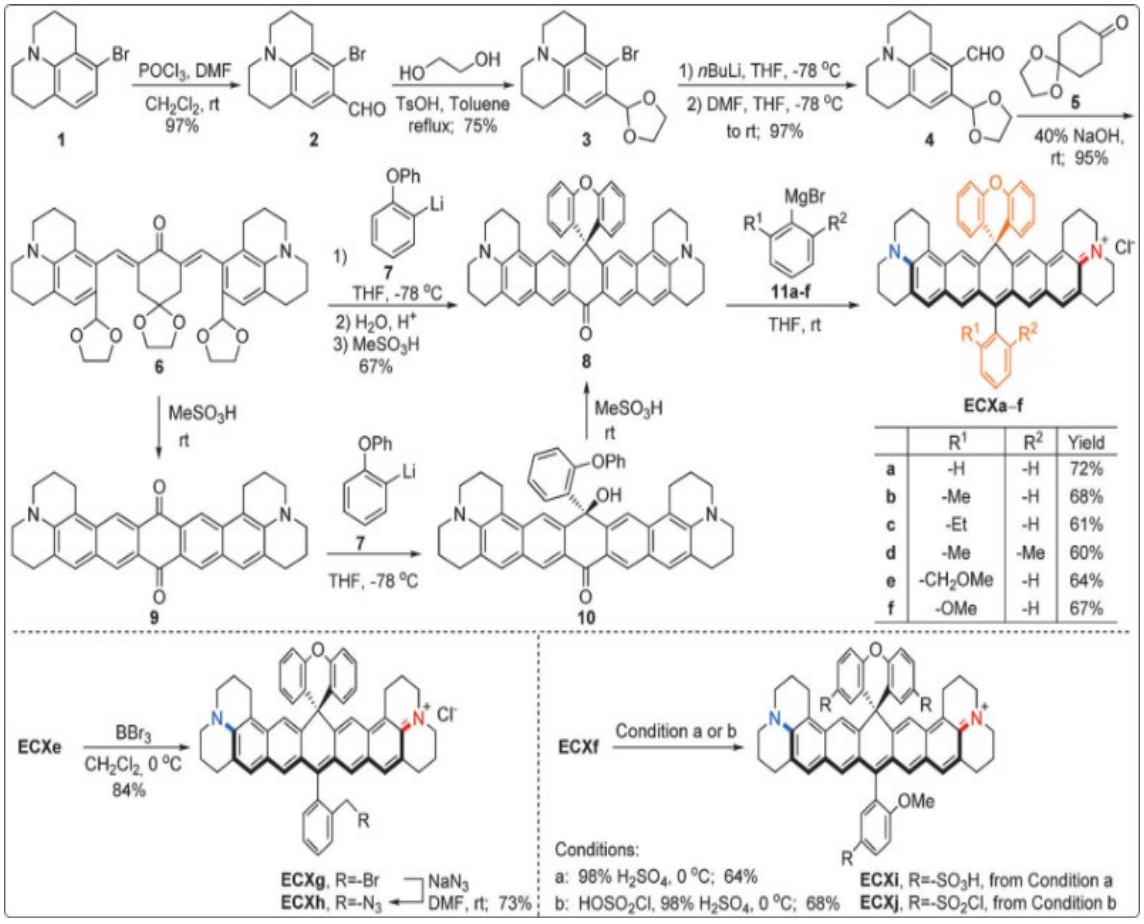

	R1	R2	Yield
a	-H	-H	72%
b	-Me	-H	68%
c	-Et	-H	61%
d	-Me	-Me	60%
e	-CH2OMe	-H	64%
f	-OMe	-H	67%

Scheme 1. Synthesis of ECX dyes. Adapted with permission from the Wiley-VCH Verlag GmbH & Co. KGaA.[34]

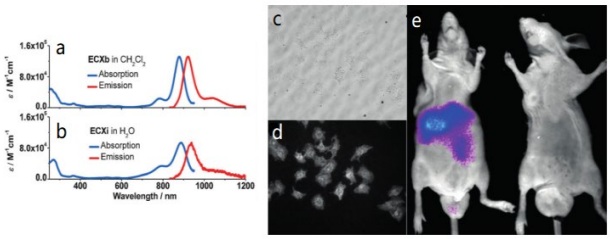

Figure 3. The absorption and emission spectra of **ECXb** (a) and **ECXi** (b), cells imaging under white-light (c) and under 808 nm excitation with **ECXb** (d) and *in vivo* imaging with (e, left) and without (e, right) **ECXb**. Adapted with permission from the Wiley-VCH Verlag GmbH & Co. KGaA.[34]

4B). **CX-1**, **CX-2**, and **CX-3** exhibit maximum absorption wavelengths at 883, 981, and 1032 nm in $CHCl_3$, respectively. The emission wavelengths in $CHCl_3$ were 920, 1089, and 1140 nm respectively with fluorescence quantum yields ranging from 0.091-0.66% in the reverse order (**CX-3** to **CX-1**). Due to the rigid polymethine chain, the **CX** dyes demonstrated great chemo- and photo-stabilities in aqueous media; however, it was presumed that the dyes aggregated in the aqueous media with increasing conjugation length leading to decreased absorbance intensity. The dyes and thier photophysical properties were recoverable with extraction into $CHCl_3$. The dyes were encapsulated into DSPE-mPEG2000 micelle used to perform high-contrast *in vivo* bioimaging at a depth of 4 mm (Figure 5A). The authors also developed a NIR-II FRET probe with the combination of **CX-1** and **CX-3** dyes for real-time monitoring of peroxynitrite (Figure 5B).

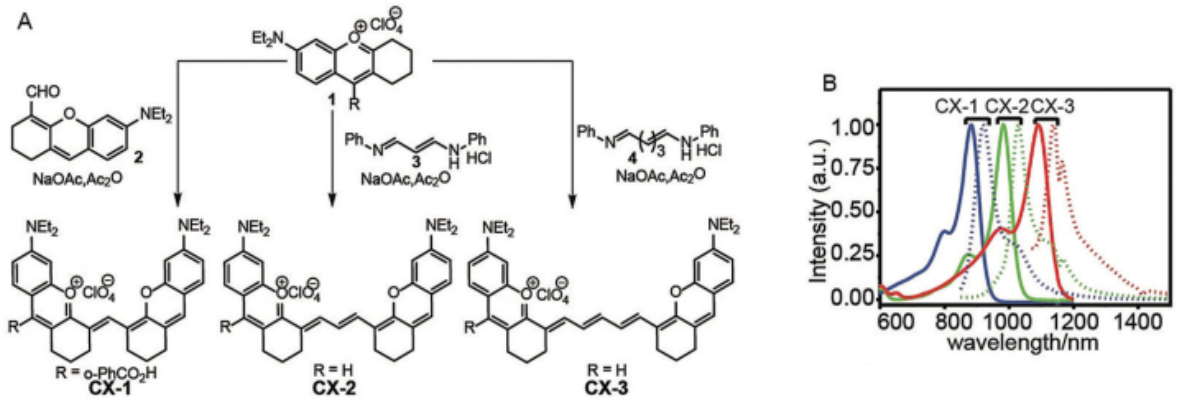

Figure 4. Synthetic routes of CX dyes (A) and normalized absorption and emission spectra of CX dyes (B). Adapted with permission from the Wiley-VCH Verlag GmbH & Co. KGaA.[35]

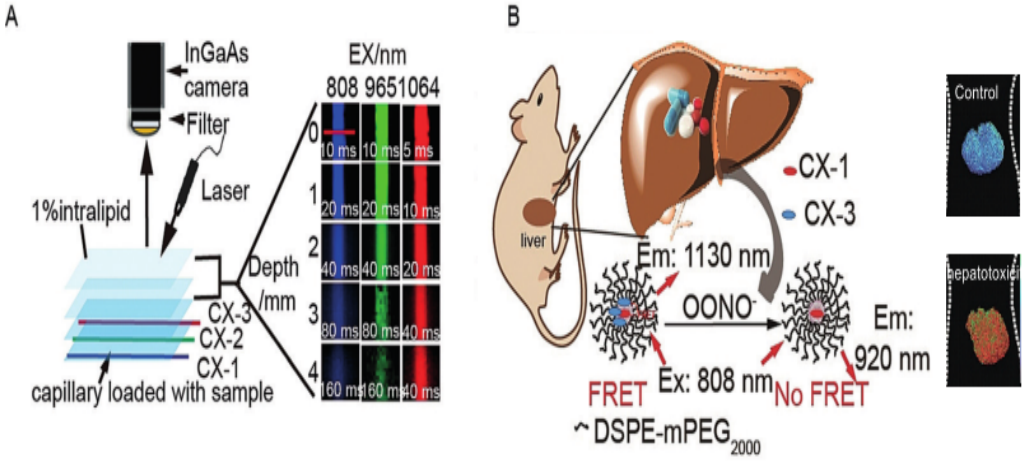

Figure 5. A) Schematic illustration of *in vitro* multicolor imaging of dyes in capillaries as a function of tissue depth under 808 nm (**CX-1**, 850LP, blue), 965 nm (**CX-2**, 1000LP, green), or 1064 nm (**CX-3,** 1100 LP, red) excitation. B) the schematic illustration of the detection mechanism of PN1100 and images of mice liver. Adapted with permission from the Wiley-VCH Verlag GmbH & Co. KGaA.[35]

The cyanine dyes are known for NIR absorption and emission. However, it is difficult to design off-on switching cyanine-based probes using the 'PET' strategy due to the relatively high-lying highest occupied molecular orbital (HOMO) energy levels.[41] By contrast, the fluorescence of rhodamine dyes can be conveniently tuned by intramolecular cyclization. Therefore, chemists have constructed a series of NIR hybrid cyanine-rhodamine dyes, which retain the advantages of both rhodamine and cyanine dyes. For example, Lin's group designed a series of rhodamines-indole/benzo[*e*]indole-based cyanine hybrid dyes;[42] however, the absorption maximum ranged from 688 nm to 728 nm, and emission maximum ranged from 721 nm to 763 nm, which are in the NIR-I region. In a similar strategy, Li *et al*., synthesized a series of rhodamine-benz[*c,d*]indole-based cyanine hybrid dyes with different lengths of polyene bonds (**Rh824**, **Rh926**, and **Rh1029**) (Figure 6A).[43] This work have successfully tuned the absorption and emission wavelengths of hybrid cyanine-rhodamine dyes from the first near-infrared window to the second near-infrared window. With the increment of each vinylene bridge unit, the absorption and emission wavelengths red-shifted around 100 nm. Consequently, **Rh824**, **Rh926,** and **Rh1029** displayed maximum absorptions at 824, 926, and 1029 nm and emissions at 872, 975, and 1093 nm, respectively. Unfortunately, the fluorescence quantum yields for **Rh824**, **Rh926**, and **Rh1029** were low, 1.30%, 0.76%, and 0.33%, respectively (Figure 6B). The low fluorescence quantum yields were ascribed to the the flexibility and *cis-trans* isomerisation of the structures. To increase their fluorescence quantum yields and water solubilities, the authors enclosed the series of dyes into phosphatidylcholine (PC) and applied them to *in vivo* vascular imaging. The NIR-II fluorophore **Rh1029-PC** demonstrated superior clarity in vascular imaging compared to its NIR-I counterpart, **Rh824-PC** (Figure 7).

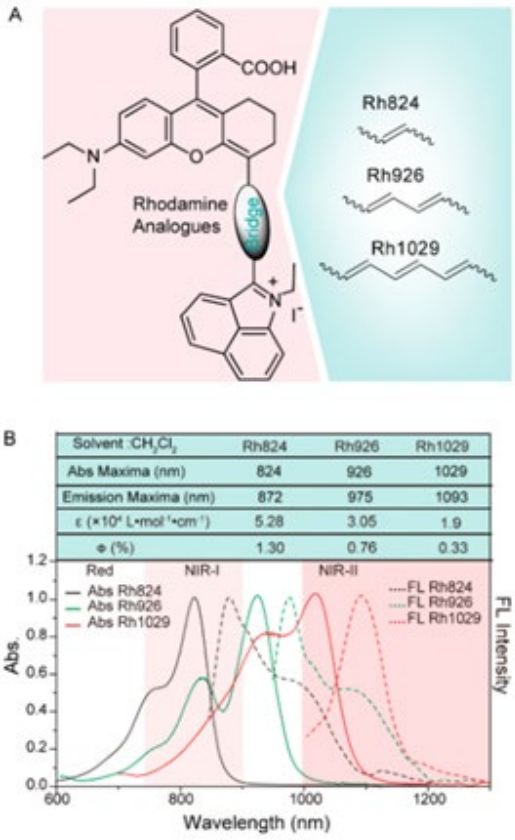

Figure 6. Molecular structures (A) and photophysical properties (B) of Rh824, Rh926, and Rh1029. Adapted with permission from (*ACS Materials Lett.* 2019, *1*, 418-424.) Copyright (2019) American Chemical Society.

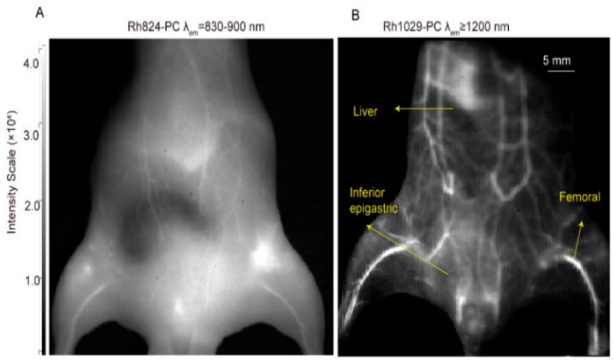

Figure 7. Images of abdomen of mice intravenously injected with (A) Rh824-PC and (B) Rh1029-PC. Adapted with permission from (*ACS Materials Lett.* 2019, *1*, 418-424). Copyright (2019) American Chemical Society.

Following a similar strategy, Zhang *et al*., also developed a new class of rhodamine analouges (**NIRII-RT3** & **NIRII-RT4**) (Figure 8A),[44] but instead of suspending the benz[*c,d*]indolium on the rhodamine skeleton as reported by Li and co-workers, they used the 1,4-diethyl-decahydro-quinoxaline (DQ) benzopyran group, which is more sterically bulky and electron-rich. The maximum absorption wavelengths of **NIRII-RT3** and **NIRII-RT4** in CH_2Cl_2 were 860 and 856 nm, respectively (Figure 8C, D). Noteworthy, the fluorophores displayed two emission peaks at 922 and 999 nm for **NIRII-RT3** and 929 and 989 nm for **NIRII-RT3** (Figure 8B) with fluorescence quantum yields of 2.03% and 1.42%, respectively. By taking advantage of the spirocyclization properties of xanthene core, the authors constructed a series of NIR-II fluorescent probes for pH, ATP, and Hg^{2+} (**NIRII-RT-pH**, **NIRII-RT-ATP**, and **NIRII-RT-Hg**) (Figure 9). So far, we have discussed the design strategies for constructing NIR-II rhodamine analogue fluorophores based

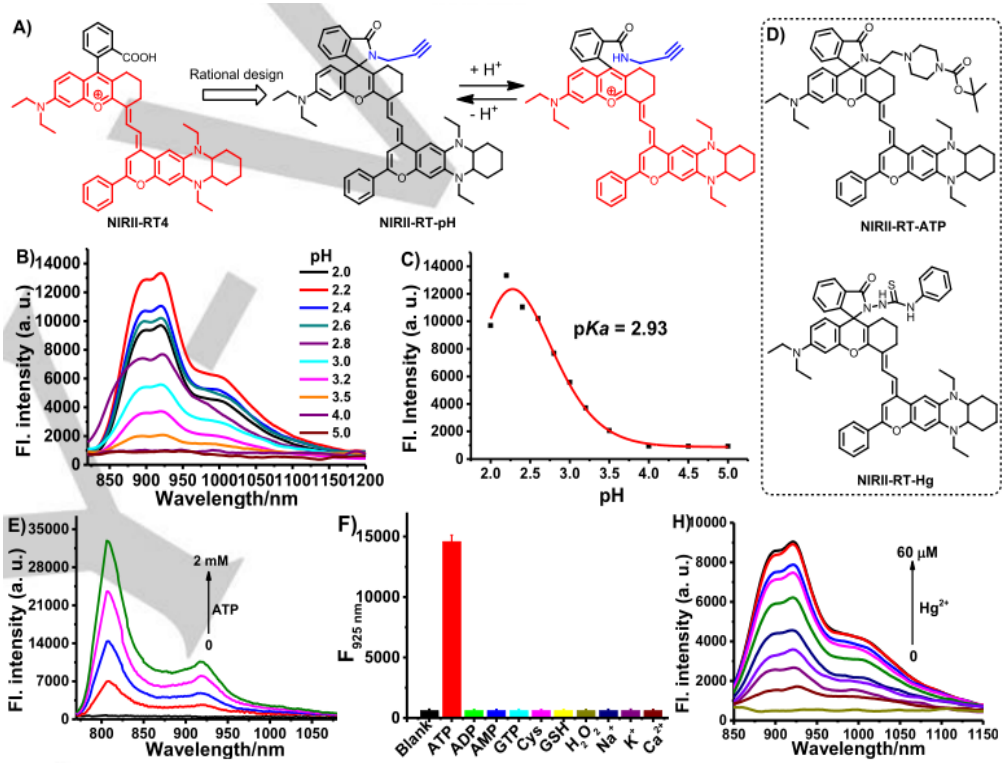

Figure 8. A) the structures of NIRII-RT3 and NIRII-RT4. (B) Emission spectrum for various NIRII dyes including NIRII-RT3 and NIRII-RT4. (C) The absorption spectra of NIRII-RT3 and (D) NIRII-RT4 in different solvents. Adapted with permission from the Wiley-VCH Verlag GmbH & Co. KGaA.[39]

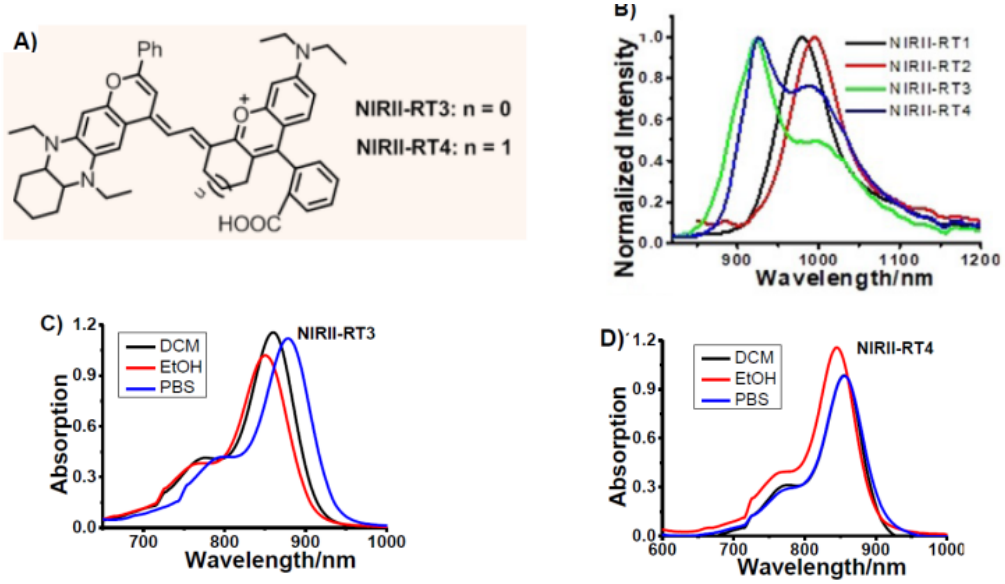

Figure 9. A) Design and synthesis of probe NIRII-RT-pH. B) Fluorescence spectra of NIRII-RT-pH at different pH values. C) The pH titration curve was plotted by NIRII-RT-pH fluorescence as a function of pH. D) Synthesis of NIR II probes NIRII-RT-ATP and NIRII-RT-Hg. E) Fluorescence spectra of NIRII-RT-ATP responding to ATP. F) Fluorescence response of NIRII-RT-ATP toward various analytes. H) Fluorescence spectra of NIRII-RT-Hg responding to Hg^{2+}. Adapted with permission from the Wiley-VCH Verlag GmbH & Co. KGaA.[39]

predominately on extending the π-conjugation of the xanthene core through vinylene bridges. However, this strategy usually requires tedious synthesis or laborious purification steps. In addition, some of the resulting dyes suffer from poor chemical and photostability, small Stokes shifts, and solvatochromic quenching in biologically relevant systems. Encouraged by the

NIR-II fluorophores with D-A-D framework as shown in Figure 1, a D-A-D type NIR-II rhodamine dye, rhodindolizine, has been prepared by the C-H bond functionalization reaction of 1-methyl-2-phenylindolizine with 3',6'-dibromofluoran (Figure 10A).[45] It is worth nothing that the synthetic strategy to prepare this dye only required two to three steps, which is far less than the other attempts to prepare NIR-II rhodamine-based dyes. The nonfluorescent rhodindolizine spirolactone product was converted to the ethyl ester of the opened formed that resulted in the fluorophore absorbing at 920 nm with a very broad emission band extending to 1400 nm with the peak at 1092 nm, which are both in the NIR II region (Figure 10B and C). Unfortunately, the quantum yield of this dye was very low (0.03%) due to its instability in aqueous media, which is similar to previous NIR-II dyes.

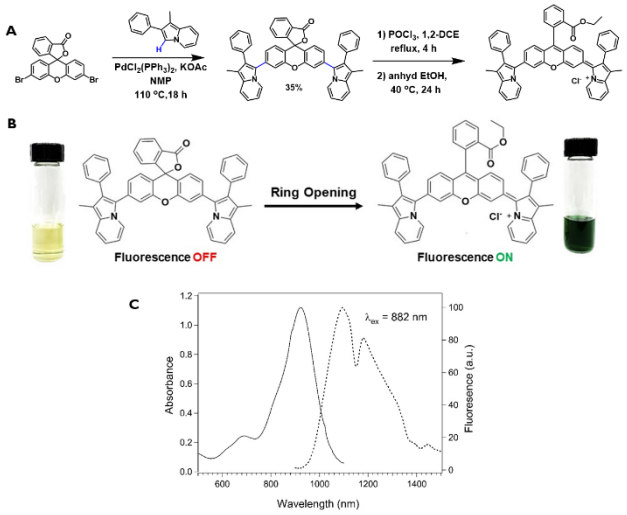

Figure 10. A) Synthesis of rhodindolizine B) Ring opening mechanism of rhodindolizine, C) Molar absorptivity and emission of rhodindolizine ethyl ester in dichloromethane. Adapted with permission from (*J. Org. Chem.* 2019, *84*, 13186-13193). Copyright (2019) American Chemical Society.

Conclusions & outlook

Overall, chemists have successfully extended the absorption and emission wavelengths of rhodamine-based dyes into the NIR-II region. The strategies include extending conjugation/hyperconjugation of the xanthene ring, hybridization with other fluorophores, and forming D-A-D type. Although the former two strategies are effective to extend the emission wavelength of these rhodamine analogues from the red to the NIR-II region, the resulting molecules usually have large molecular weight, low solubility, and poor stability in biologically relevant media. By contrast, the D-A-D type rhodamine dyes developed by us have relatively smaller molecular weight. Besides the above strategies, there is another way to shift the absorption and emission wavelengths of rhodamine to obtain larger bathochromic shifts. Specifically, replacing the central oxygen atom with other elements such as Si,[33] P,[32] S[30] and Se[30] are common strategies to elicit a pronounced bathochromic shift in λ_{ex} and λ_{em}. Although this strategy presently only results in NIR-I dyes, we envision that combining this strategy with D-A-D approach will generate longer absorption and emission wavelengths than each single strategy alone. In our group, we are currently working on incorporating Si, and P into our D-A-D dyes to obtain dyes with λ_{abs} and λ_{em} well into the NIR-II region with good solubility, good stability in biological media, and high quantum yield for use in bioimaging applications.

The photophysical properties of NIR-II fluorophores of rhodamine analogues have been presented. Many of these fluorophores demonstrate good photophysical performance, deep tissue penetration, and higher resolution *in vivo* imaging compared to their NIR-I counterparts. However, NIR-II rhodamine-based fluorophores are still in their infancy, with many limitations to overcome. For example, rhodamine-based fluorophores with NIR-II absorption and maximum emission wavelengths beyond 1000 nm are still lacking and those that possess these wavelengths have low quantum yields. Besides, the NIR-II rhodamine analogues usually adopt spirolactone form in nature, and opening of the lactone ring is sometimes difficult, which hampers their development as off-on NIR-II fluorescence probes. Finally, synthesis of many of these fluorophores require lengthy synthetic steps, which adds to the cost of their development. Consequently, continued studies are needed to address these limitations and develop highly emissive NIR-II rhodamine-based probes to meet clinical needs.

A promising future research focus would be to expand the diversity of NIR-II rhodamine-based dyes and their applications as NIR-II dyes. Fluorescence imaging (FI) possesses high spatiotemporal resolution for cells imaging and thereby makes it easier to monitor movement, location, and concentration of biomolecules at subcellular levels.[46] However, the photostability of the dyes limits their further application in dynamic and long-term monitoring analysts in living systems.[47] On the other hand, photoacoustic imaging (PA) is an emerging technique capable of providing anatomical, functional, and molecular properties of biological tissue with high resolution.[48] Thus, it offers the

opportunity to provide multimodal imaging with FI. This approach is always attractive and desirable, since it can combine the strengths of several imaging modalities and is able to characterize biological tissue more completely, thus offering the possibility of precision diagnosis of diseases. Thus, developing NIR-II rhodamine-based dual-modality (FI/PA) or even multimodal (FI/PA/MRI) imaging agents should be another focus of future research. Finally, by taking advantage of NIR-II excitation (deep penetration), development of NIR-II rhodamine-based photosensitizers for photodynamic therapy or photothermal therapy will be highly desired for treatment of deep-seated tumors. [49-51] Therefore, there is still ample scope for the development of new NIR-II rhodamine dyes.

Acknowledgements

We are grateful for the financial support from the National Science Foundation for award OIA-1757220 and under the Center for Chemical Innovation in Selective C − H Functionalization (CHE-1700982).

Conflicts of interest

There are no conflicts to declare.

Keywords: Rhodamine • NIR-II • Xanthene • Imaging • Fluorescent probes

References

[1] D. Wu, A. C. Sedgwick, T. Gunnlaugsson, E. U. Akkaya, J. Yoon and T. D. James, Fluorescent chemosensors: the past, present and future, *Chem. Soc. Rev.,* 2017, **46**, 7105-7123.
[2] Y. Lv, D. Cheng, D. Su, M. Chen, B. Yin, L. Yuan and X. Zhang, Visualization of oxidative injury in the mouse kidney using selective superoxide anion fluorescent probes, *Chem. Sci.*, 2018, **9**, 7606-7613.
[3] J. Ning, W. Wang, G. Ge, P. Chu, F. Long, Y. Yang, Y. Peng, L. Feng, X. Ma and T. James, Target enzyme-activated two-photon fluorescent probes: a case study of CYP_3A_4 using a two-dimensional design strategy, *Angew. Chem. Int. Ed.*, 2019, **58**, 9959-9963.
[4] H.-S. Peng and D. T. Chiu, Soft fluorescent nanomaterials for biological and biomedical imaging, *Chem. Soc. Rev.*, 2015, **44**, 4699-4722.
[5] S. Zhu, Z. Hu, R. Tian, B. C. Yung, Q. Yang, S. Zhao, D. O. Kiesewetter, G. Niu, H. Sun, A. L. Antaris and X. Chen, Repurposing cyanine NIR-I dyes accelerates clinical translation of near-Infrared-Ⅱ (NIR-Ⅱ) bioimaging, *Adv. Mater.,* 2018, **30**, 1802546.
[6] B. Li, L. Lu, M. Zhao, Z. Lei and F. Zhang, An efficient 1064 nm NIR-II excitation fluorescent molecular dye for deep-tissue high-resolution dynamic bioimaging, *Angew. Chem. Int. Ed.*, 2018, **57**, 7483-7487.
[7] F. Ding, Y. Zhan, X. Lu and Y. Sun, Recent advances in near-infrared II fluorophores for multifunctional biomedical imaging, *Chem. Sci.*, 2018, **9**, 4370-4380.
[8] G. Hong, A. L. Antaris, and H. Dai, Near-infrared fluorophores for biomedical imaging, *Nat. Bio. Eng.* 2017, **1**, 10.
[9] C. Li, G. Chen, Y. Zhang, F. Wu and Q. Wang, Advanced fluorescence imaging technology in the near-Infrared-II window for biomedical applications, *J. Am. Chem. Soc.*, 2020, **142**, 14789-14804.
[10] Y. Chen, Y. Wang, Y. Yang, Y. Li, Y. Wang, G. Wang, T. James, X. Xuan, H. Zhang and Y. Liu, A molecular-logic gate for COX-2 and NAT based on conformational and structural changes: visualizing the progression of liver disease, *Chem. Sci.*, 2020, **11**, 6209-6216.
[11] Y. Chen, Y. Liu, S. Lu, S. Ye, H. Gu, J. Qiang, Y. Li and X. Chen, Photostimulated spiropyran for instantaneous visualization of thermal field distribution and flow pattern, *J. Am. Chem. Soc.*, 2020, **142**, 20066-20070.
[12] J. Liu, Y. Yang, K. Wang, G. Wang, C. Shen, Y. Chen, Y. Liu, T. James, K. Jiang and H. Zhang, Activation and monitoring of mtDNA damage in cancer cells via the “proton-triggered“ decomposition of an ultrathin nanosheet, *ACS Appl. Mater. Interfaces*, 2021, **13**, 3669-3678.
[13] S. Zhu, R. Tian, A. L. Antaris, X. Chen and H. Dai, Near-Infrared-II molecular dyes for cancer imaging and surgery, *Adv. Mater.,* 2019, **31**, 1900321.
[14] Z. Lei and F. Zhang, Molecular engineering of NIR-II fluorophores for improved biomedical detection, *Angew. Chem. Int. Ed.,* DOI: 10.1002/anie.202007040.
[15] F. Ding, Y. Zhan, X. Lu and Y. Sun, Recent advances in near-infrared II fluorophores for multifunctional biomedical imaging, *Chem. Sci.,* 2018, **9**, 4370-4380.
[16] S. He, J. Song, J. Qu and Z. Cheng, Crucial breakthrough of second near-infrared biological window fluorophores: design and synthesis toward multimodal imaging and theranostics, *Chem. Soc. Rev.*, 2018, **47**, 4258-4278.
[17] Y. Su, B. Yu, S. Wang, H. Cong and Y. Shen, NIR-II bioimaging of small organic molecule, *Biomaterials,* 2021, **271**, 120717.
[18] W. Xu, D. Wang and B. Tang, NIR-II AIEgens: A win-win integration towards bioapplications, *Angew. Chem. Int. Ed.,* 2021, **60**, 7476-7487.
[19] X. Chen, T. Pradhan F. Wang, J. S. Kim and J. Yoon, Fluorescent chemosensors based on spiroring-opening of xanthenes and related derivatives, *Chem. Rev.,* 2012, **112**, 1910-1956.
[20] H. N. Kim, M. H. Lee, H. J. Kim, J. S. Kim and J. Yoon, A new trend in rhodamine-based chemosensors: application of spirolactam ring-opening to sensing ions, *Chem. Soc. Rev.,* 2008, **37**, 1465-1472.
[21] Y. Yang, Q. Zhao, W. Feng and F. Li, Luminescent chemodosimeters for bioimaging, *Chem. Rev.,* 2012, **113**, 192-270.
[22] G. Y. Wiederschain, The molecular probes handbook. A guide to fluorescent probes and labeling technologies, *Biochemistry (Moscow)*, 2011, **76**, 1276-1276.
[23] L. Yuan, W. Lin, K. Zheng, L. He and W. Huang, Far-red to near infrared analyte-responsive fluorescent probes based on organic fluorophore platforms for fluorescence imaging, *Chem. Soc. Rev.*, 2013, **42**, 622-661.
[24] C. Staudinger and S. M. Borisov, Long-wavelength analyte-sensitive luminescent probes and optical (bio)sensors, *Methods and Applications in Fluorescence,* 2015, **3**, 042005.
[25] S. A. Hilderbrand and R. Weissleder, Near-infrared fluorescence: application to *in vivo* molecular imaging, *Curr. Opin. Chem. Biol.,* 2010, **14**, 71-79.
[26] R. Weissleder, A clearer vision for *in vivo* imaging, *Nat. Biotechnol.,* 2001, **19**, 316-317.
[27] R. Weissleder and V. Ntziachristos, Shedding light onto live molecular targets, *Nat. Med.,* 2003, **9**, 123-128.
[28] L. Wang, W. Du, Z. Hu, K. Uvdal, L. Li and W. Huang, Hybrid rhodamine fluorophores in the visible/NIR region for biological imaging, *Angew. Chem. Int. Ed.,* 2019, **58**, 14026-14043.
[29] J. Arden-Jacob and K. H. Drexhage, New fluorescent markers for the red region, *Spectrochimica Acta Part A,* 2001, **57**, 2271-2283.
[30] M. R. Detty, P. N. Prasad, D. J. Donnelly, T. Ohulchanskyy, S. L. Gibson and R. Hilf, Synthesis, properties, and photodynamic properties *in vitro* of heavy-chalcogen analogues of tetramethylrosamine, *Bioorgan. Med. Chem.*, 2004, **12**, 2537-2544.
[31] J. Liu, Y. Sun, H. Zhang, H. Shi, Y. Shi and W. Guo, Sulfone-rhodamines: a new class of near-infrared fluorescent dyes for bioimaging, *ACS Appl. Mater. Inter.*, 2016, **8**, 22953-22962.

[32] X. Zhou, R. Lai, J. R. Beck, H. Li and C. I. Stains, Nebraska Red: a phosphinate-based near-infrared fluorophore scaffold for chemical biology applications, *Chem. Commun.,* 2016, **52**, 12290-12293.
[33] Y. Koide, Y. Urano, K. Hanaoka, T. Terai and T. Nagano, Evolution of group 14 rhodamines as platforms for near-infrared fluorescence probes utilizing photoinduced electron transfer, *ACS Chem. Biol*., 2011, **6**, 600-608.
[34] Y. Koide, M. Kawaguchi, Y. Urano, K. Hanaoka, T. Komatsu, M. Abo, T. Terai and T. Nagano, A reversible near-infrared fluorescence probe for reactive oxygen species based on Te-rhodamine, *Chem. Commun.*, 2012, **48**, 3091-3093.
[35] J. Li and K. Pu, Development of organic semiconducting materials for deep-tissue optical imaging, phototherapy and photoactivation, *Chem. Soc. Rev.,* 2019, **48**, 38-71.
[36] A. M. Smith, M. C. Mancini and S. Nie, Bioimaging: second window for *in vivo* imaging, *Nat. Nanotechnol.,* 2009, **4**, 710-711.
[37] J. B. Grimm, A. J. Sung, W. R. Legant, P. Hulamm, S. M. Matlosz, E. Betzig and L. D. Lavis, Carbofluoresceins and carborhodamines as scaffolds for high-contrast fluorogenic probes, *ACS Chem. Biol.,* 2013, **8**, 1303-1310.
[38] H. Sasaki, K. Hanaoka, Y. Urano, T. Terai, and T. Nagano, Design and synthesis of a novel fluorescence probe for Zn2+ based on the spirolactam ring-opening process of rhodamine derivatives, *Bioorg. Med. Chem.*, 2011, **19**, 1072-1078.
[39] Z. Lei, X. Li, X. Luo, H. He, J. Zheng, X. Qian and Y. Yang, Bright, stable, and biocompatible organic fluorophores absorbing/e mitting in the deep near-infrared spectral region, *Angew. Chem. Int. Ed.*, 2017, **56**, 1-6.
[40] Z. Lei, C. Sun, P. Pei, S. Wang, D. Li, X. Zhang and F. Zhang, Stable, wavelength-tunable fluorescent dyes in the NIR-II region for *in vivo* high-contrast bioimaging and multiplexed biosensing, *Angew. Chem. Int. Ed.*, 2019, **58**, 8166-8171.
[41] F. Yu, P. Li, G. Li, G. Zhao, T. Chu and K. Han, A near-IR reversible fluorescent probe modulated by selenium for monitoring peroxynitrite and imaging in living cells, *J. Am. Chem. Soc.* 2011, **133**, 11030-11033.
[42] L. Yuan, W. Lin, Y. Yang and H. Chen, A unique class of near-infrared functional fluorescent dyes with carboxylic-acid-modulated fluorescence ON/OFF switching: rational design, synthesis, optical properties, theoretical calculations, and applications for fluorescence imaging in living animals, *J. Am. Chem. Soc.*, 2012, **134**, 1200-1211.
[43] Y. Shi, W. Yuan, Q. Liu, M. Kong, Z. Li, W. Feng, K. Hu and F. Li, Development of polyene-bridged hybrid rhodamine fluorophores for high-resolution NIR-II imaging, *ACS Materials Lett.*, 2019, **1**, 418-424.
[44] T. Ren, Z. Wang, Z. Xiang, P. Lu, H. Lai, L. Yuan, X. Zhang and W. Tan, A general strategy for development of activatable NIR-II fluorescent probes for *in vivo* high-contrast bioimaging, *Angew. Chem. Int. Ed.,* 2021, **60**, 800-805.
[45] C. S. L. Rathnamalala, J. N. Gayton, A. L. Dorris, S. A. Autry, W. Meador, N. I. Hammer, J. H. Delcamp and C. N. Scott, Donor-acceptor-donor NIR II emissive rhodindolizine dye synthesized by C-H bond functionalization, *J. Org. Chem.,* 2019, **84**, 13186-13193.
[46] P. Ou, R. Zhang, Z. Liu, X. Tian, G. Han, B. Liu, Z. Hu and Z. Zhang, Gasotransmitter regulation of phosphatase activity in live cells studied by three-channel imaging correlation, *Angew. Chem. Int. Ed.,* 2019, **58**, 2261-2265.
[47] W. Zhang, P. Li, F. Yang, X. Hu, C. Sun, W. Zhang, D. Chen and B. Tang, Dynamic and reversible fluorescence imaging of superoxide anion fluctuations in live cells and *in vivo*, *J. Am. Chem. Soc.,* 2013, **135**, 14956-14959.
[48] L. Nie and X. Chen, Structural and functional photoacoustic molecular tomography aided by emerging contrast agents, *Chem. Soc. Rev.*, 2014, **43**, 7132-7170.
[49] L. Li, C. Shao, T. Liu, Z. Chao, H. Chen, F. Xiao, H. He, Z. Wei, Y. Zhu, H. Wang, X. Zhang, Y. Wen, B. Yang, F. He and L. Tian, An NIR-II-emissive photosensitizer for hypoxia-tolerant photodynamic theranostics, *Adv. Mater.*, 2020, **32**, e2003471.
[50] L. Jin, S. Shen, Y. Huang, D. Li and X. Yang, Corn-like Au/Ag nanorod-mediated NIR-II photothermal/photodynamic therapy potentiates immune checkpoint antibody efficacy by reprogramming the cold tumor microenvironment, *Biomaterials*, 2021, **268**, 120582.
[51] Y. Xu, Y. Zhang, J. Li, J. An, C. Li, S. Bai, A. Sharma, G. Deng, J. Kim and Y. Sun, NIR-II emissive multifunctional AIEgen with single laser-activated synergistic photodynamic/photothermal therapy of cancers and pathogens, *Biomaterials*, 2020, **259**, 120315.

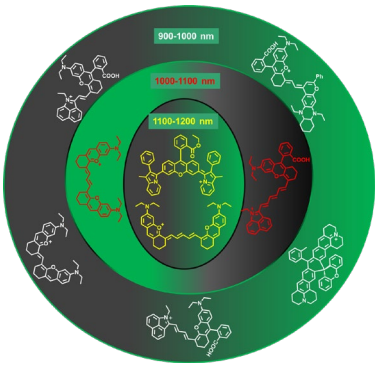

This mini-review summarizes the strategies to make NIR-II (900-1700 nm) fluorophores based on the rhodamine core, which furnish low background autofluorescence, reduced photon scattering, and higher resolution at the millimeter depth for bioimaging. These dyes are superior to rhodamine-based fluorophores in the visible (400-700 nm) and NIR-I (700-900 nm) regions.